An engineering approach to study the effect of saturation-dependent capillary diffusion on radial Buckley-Leverett flow

Meulenbroek, Bernard; Khoshnevis Gargar, Negar; Bruining, Hans

DOI
10.1007/s10596-020-09993-y

Publication date
2020

Document Version
Final published version

Published in
Computational Geosciences

Citation (APA)
Meulenbroek, B., Khoshnevis Gargar, N., & Bruining, H. (2020). An engineering approach to study the effect of saturation-dependent capillary diffusion on radial Buckley-Leverett flow. *Computational Geosciences*, *25*(2), 637-653. https://doi.org/10.1007/s10596-020-09993-y

Computational Geosciences
https://doi.org/10.1007/s10596-020-09993-y

An engineering approach to study the effect of saturation-dependent capillary diffusion on radial Buckley-Leverett flow

Bernard Meulenbroek[1] · **Negar Khoshnevis Gargar**[2] · **Hans Bruining**[3]

Received: 12 March 2019 / Accepted: 6 August 2020

Abstract

1D water oil displacement in porous media is usually described by the Buckley-Leverett equation or the Rapoport-Leas equation when capillary diffusion is included. The rectilinear geometry is not representative for near well oil displacement problems. It is therefore of interest to describe the radially symmetric Buckley-Leverett or Rapoport-Leas equation in cylindrical geometry (radial Buckley-Leverett problem). We can show that under appropriate conditions, one can apply a similarity transformation $(r, t) \rightarrow \eta = r^2/(2t)$ that reduces the PDE in radial geometry to an ODE, even when capillary diffusion is included (as opposed to the situation in the rectilinear geometry (Yortsos, Y.C. (Phys. Fluids 30(10),2928–2935 1987)). We consider two cases (1) where the capillary diffusion is independent of the saturation and (2) where the capillary diffusion is dependent on the saturation. It turns out that the solution with a constant capillary diffusion coefficient is fundamentally different from the solution with saturation-dependent capillary diffusion. Our analytical approach allows us to observe the following conspicuous difference in the behavior of the dispersed front, where we obtain a smoothly dispersed front in the constant diffusion case and a power-law behavior around the front for a saturation-dependent capillary diffusion. We compare the numerical solution of the initial value problem for the case of saturation-dependent capillary diffusion obtained with a finite element software package to a partially analytical solution of the problem in terms of the similarity variable η.

Keywords Radial Buckley-Leverett flow · Similarity transformation · Saturation dependent capillary diffusion · Power law behavior

1 Introduction

Water drive recovery of oil is one of the most important secondary recovery methods. The displacement in rectilinear (1D) geometry can be described by the Buckley-Leverett (BL) model. The BL model disregards capillary diffusion but uses a saturation-dependent fractional flow to model the water and oil flux functions. To obtain a unique solution, it is necessary to consider the limit of vanishing capillary diffusion ([6, 9, 10, 14]), leading to the entropy condition. The solution in 1D consists of a rarefaction wave, followed by a shock to a constant state. When capillary diffusion is included, the problem is known as the Rapoport-Leas (RL) equation [11]. In this case, the shock is replaced by a smooth saturation profile. Understanding of the displacement process is enhanced when considering radial geometries. King [3] describes a Buckley-Leverett problem with capillary diffusion through a cylindrical tube in the axial direction. Yortsos [16] presents an analytical solution to the 1D Rapoport-Leas equation (Buckley-Leverett + capillary diffusion), by specially adapting the constitutive relations (relative permeability and capillary pressure), such that an exact solution can be obtained [16].

In the absence of diffusion, the radial problem is similar to the 1D problem, where the solution again consists of a rarefaction wave and a shock connected to the constant initial state. As in the 1D case, the shock saturation can be determined by Welge's tangent construction (see Appendices 1, 2 and [14]). However, the radial saturation profile cannot be approximated by the linear saturation profile because this leads to a violation of mass conservation and thus to an incorrect prediction of the shock position (see

✉ Bernard Meulenbroek
b.j.meulenbroek@tudelft.nl

[1] Delft University of Technology, Delft Institute of Applied Mathematics, Mekelweg 4, 2628, CD, Delft, The Netherlands

[2] Deltares, Unit Geo-Engineering, Boussinesqweg 1, 2629, HV Delft, The Netherlands

[3] Delft University of Technology, Department of Geotechnology, Stevinweg 1, 2628, CN, Delft, The Netherlands

Published online: 29 August 2020

[8]). Capillary diffusion can be straightforwardly included in the cylindrical model. This model can be solved using a finite element package ([1]), if the capillary diffusion is taken large enough. We solve it using COMSOL as detailed in Section 4. The numerical results indicate that the shock is replaced by a continuous curve that follows a power-law behavior: continuous but not differentiable at the toe where $S_w = S_{wc}$. A larger capillary diffusion leads to broader fronts. We also studied the problem using a similarity transformation $(r, t) \rightarrow r^2/(2t = \eta)$. Contrary to the 1D case, the model equations including the capillary diffusion term can be expressed entirely in terms of η. This leads to a system of coupled ODEs for the saturation and pressure. In the incompressible case, the saturation equation decouples from the pressure equation. We obtain a second-order ODE for the saturation [15] and an ODE for the pressure with saturation-dependent coefficients. Yortsos [15] studies the stability of the saturation profile in two asymptotic cases. Yortsos [15] did not consider explicit solutions for general cases of saturation-dependent capillary diffusion in a radially symmetric Buckley-Leverett problem. In this manuscript, we carry out an extension of the work by Yortsos in the sense that we consider generic saturation-dependent capillary diffusion. A second innovation is that we consider explicit solutions for S_w and more importantly for the pressure, which can be helpful when these solutions are applied for the pressure build-up. We follow the approach due to Yortsos, where we determine self-similar solutions for cases of small well radii and long-time behavior. Furthermore, also in Yortsos, we approximate the location of the boundary condition on the injection well by shifting the injection well boundary to the origin of the computational domain. This approximation is accurate moderately far from the well and for the long-time behavior. Our more general approach can be used to gain quick insight into the relation between several input and output parameters, as well as for testing of numerical simulators.

The model equations are presented in Section 2 and analyzed in Section 3 using our similarity transformation. The case with a saturation-dependent capillary diffusion is solved with a combination of analytical and numerical methods in Section 3.1. The case with small, but constant, capillary diffusion is solved in Section 3.3 using the method of matched asymptotic expansions. Numerical results are presented in Section 4 and subsequently discussed in Section 5. We end the paper with some conclusions. Although most of the theory in the Appendices is well-known, we have added the Appendices for the convenience of the reader who needs to recap this theory.

We finally note that the current manuscript is meant to have a descriptive nature, rather than being mathematically rigorous.

2 Mathematical model

In this section, we formulate our model equations in dimensionless form; we use capital letters or variables with superscript $\sim$ for (in)dependent variables with dimensions, small letters for dimensionless (in)dependent variables, and we use the subindex c for characteristic scales. Notice that only three scales need to be chosen: length, time, and pressure: ρ_c will drop out entirely because gravity is neglected.

The mass conservation equation for water reads in full-dimensional form:

$$\varphi \frac{\partial}{\partial T}(\rho_w S_w) + \frac{1}{R}\frac{\partial}{\partial R}(U_w R \rho_w) = 0. \tag{1}$$

The term $U_w \frac{\partial \rho_w}{\partial R}$ is proportional to the square of the pressure gradient $\frac{\partial p_w}{\partial R}$ which is small and can thus be neglected (since $U_w \sim \frac{\partial p_w}{\partial R}$ and $\frac{\partial \rho_w}{\partial R} = \frac{d\rho_w}{dp_w}\frac{\partial p_w}{\partial R}$ see [2], Ch. 5, equation (5.18)).

Furthermore, we divide by ρ_w and we obtain:

$$\varphi \frac{\partial S_w}{\partial T} + \varphi \frac{S_w}{\rho_w}\frac{\partial \rho_w}{\partial T} + \frac{1}{R}\frac{\partial}{\partial R}(U_w R) = 0. \tag{2}$$

Similarly, we find for oil (neglecting $\frac{\partial \rho_o}{\partial R}$):

$$\varphi \frac{\partial S_o}{\partial T} + \varphi \frac{S_o}{\rho_o}\frac{\partial \rho_o}{\partial T} + \frac{1}{T}\frac{\partial}{\partial T}(U_o R) = 0. \tag{3}$$

Adding (2) and (3) yields:

$$\frac{1}{R}\frac{\partial}{\partial R}(R U_{tot}) + \varphi \frac{S_o}{\rho_o}\frac{\partial \rho_o}{\partial T} + \varphi \frac{S_w}{\rho_w}\frac{\partial \rho_w}{\partial T} = 0, \tag{4}$$

where $U_{tot} = U_w + U_o$. Using isothermal compressibilities for oil and water, we have:

$$\frac{1}{\rho_o}\frac{\partial \rho_o}{\partial T} = \frac{1}{\rho_o}\frac{\partial \rho_o}{\partial P_o}\frac{\partial P_o}{\partial T} = \tilde{c}_o \frac{\partial P_o}{\partial t}, \tag{5}$$

where $\frac{1}{\rho_o}\frac{\partial \rho_o}{\partial P_o} = \tilde{c}_o$. We finally obtain:

$$\frac{1}{R}\frac{\partial}{\partial R}(R U_{tot}) + \varphi S_o \tilde{c}_o \frac{\partial P_o}{\partial T} + \varphi S_w \tilde{c}_w \frac{\partial P_w}{\partial T} = 0. \tag{6}$$

Furthermore, we use Darcy's law, i.e.:

$$U_w = -\frac{k}{\mu_w} k_{rw} \frac{dP_w}{dR} = -\Lambda_w \frac{dP_w}{dR},\ U_o = -\frac{k}{\mu_o} k_{ro} \frac{dP_o}{dR} = -\Lambda_o \frac{dP_o}{dR}, \tag{7}$$

where we used the mobility

$$\Lambda_i = \frac{k}{\mu_i} k_{ri}. \tag{8}$$

This means that we find:

$$U_{tot} = -\Lambda_w \frac{\partial P_w}{\partial R} - \Lambda_o \frac{\partial P_o}{\partial R},\ \Lambda_{tot} = \Lambda_w + \Lambda_o. \tag{9}$$

The capillary pressure $P_{cap} = P_o - P_w$ can be used to express U_w in terms of U_{tot}, i.e.:

$$U_w = f_w U_{tot} + f_w \Lambda_o \frac{\partial P_{cap}}{\partial R} = f_w U_{tot} - \tilde{D}_{cap} \frac{\partial S_w}{\partial R}, \quad (10)$$

where we used $f_w = \frac{\Lambda_w}{\Lambda_{tot}}$ and the capillary diffusion coefficient $\tilde{D}_{cap} = -\frac{\Lambda_w \Lambda_o}{\Lambda_{tot}} \frac{dP_{cap}}{dS_w}$. This can be substituted in Eq. 2 to obtain:

$$\varphi \frac{\partial S_w}{\partial T} + \varphi S_w \tilde{c}_w \frac{\partial P_w}{\partial T} + \frac{1}{R} \frac{\partial}{\partial R} (R f_w U_{tot}) + \frac{1}{R} \frac{\partial}{\partial R} \left(-R \tilde{D}_{cap} \frac{\partial S_w}{\partial R} \right) = 0. \quad (11)$$

The model is supplemented with appropriate initial and boundary conditions in Section 2.1; constitutive relations for the mobilities and capillary pressure are given in Section 2.2. The relevant scales for time, length, and pressure (t_c, r_c and p_c) are discussed in Section 2.3 and used to rewrite the model equations in dimensionless form in Section 2.4. We end with a summary of the model equations for easy reference in Section 2.5.

2.1 Initial and boundary conditions

Inflow of pure water at a given rate yields boundary conditions for S_w and RU_{tot} at the inlet $R = R_w$, i.e.:

$$S_w = 1 \text{ at } R = R_w, \quad (12)$$

$$RU_{tot} = \frac{Q_{inj}}{2\pi H} \text{ at } R = R_w \quad (13)$$

Initially in the compressible case, we have oil at constant pressure, which yields initial conditions for S_w and P_w at $T = 0$, i.e.:

$$S_w = S_{wc}, \quad \text{at } T = 0 \quad (14)$$

$$P_w = P_{w0}, \quad \text{at } T = 0. \quad (15)$$

The initial water pressure is some constant. Due to the gauge invariance, the specific value of the constant does not matter. In the incompressible case, we only have an initial condition for S_w; however, the time dependence of the pressure enters through the time-dependent saturation profile, but not due to an initial pressure condition for the incompressible case. Notice that Eq. 42 requires a numerical boundary condition for S_w as $R \to \infty$; we set:

$$S_w \to S_{wc} \text{ as } R \to \infty \quad (16)$$

as water travels a finite distance in a finite time, which means that the water saturation effectively remains at its initial value as $R \to \infty$.

Table 1 Parameters in the constitutive relations

n_w	4
$k_{rw,0}$	0.2
S_{wc}	0.1
n_o	1.8
$k_{ro,0}$	0.93

2.2 Overview of the constitutive relations

Water mobility:

$$\Lambda_w = \frac{k}{\mu_w} k_{rw} = \frac{k}{\mu_w} k_{rw,0} \left(\frac{S_w - S_{wc}}{1 - S_{wc}} \right)^{n_w}. \quad (17)$$

Oil mobility:

$$\Lambda_o = \frac{k}{\mu_o} k_{ro} = \frac{k}{\mu_o} k_{ro,0} \left(\frac{1 - S_w}{1 - S_{wc}} \right)^{n_o}. \quad (18)$$

Total mobility and fractional flows:

$$\Lambda_{tot} = \Lambda_w + \Lambda_o, \quad f_w = \frac{\Lambda_w}{\Lambda_{tot}}, \quad f_o = \frac{\Lambda_o}{\Lambda_{tot}}. \quad (19)$$

Capillary pressure:

$$P_{cap} = P_{cb} \left(\frac{S_w - S_{wc}}{1 - S_{wc}} \right)^{\frac{-1}{\lambda}}, \quad \lambda = \frac{2}{n_w - 3}. \quad (20)$$

We will use the dimensionless parameters from Table 1 in the constitutive relations.

2.3 Length scales and parameters

We must now assign the reference values, t_c, r_c, and p_c. Our interest is in well testing and therefore we choose for the time scale of interest t_c = one day $= 8.64 \times 10^4$ s. From this, we can derive the characteristic radius r_c around the well that will be affected during the well test:

$$r_c = \sqrt{\frac{Q_{inj} t_c}{2\pi H}}. \quad (21)$$

Note that due to this specific choice, numeric constants are absorbed in the length scale which will simplify our expression $ru_{tot} = 1$ in Section 3.2.

The reference pressure can be obtained independent of our choice of t_c from:

$$p_c = \frac{\mu_w}{k} \frac{Q_{inj}}{2\pi H}. \quad (22)$$

In summary:

- Timescales in days, $t_c = 1$ day $= 0.864 \cdot 10^5$ seconds
- Length scale $r_c = \sqrt{\frac{Q_{inj} t_c}{2\pi H}} = 0.73$[m][1]

[1] Note that with the chosen characteristic time and the given injection rate, the affected domain of interest is about fourteen well radii in one day

- Pressure scale $p_c = \frac{\mu_w}{k}\frac{Q_{inj}}{2\pi H} = 0.61[bar]$,

where the physical constants are given in Table 2.

2.4 Model equations in dimensionless form

Using $R = r\ r_c$, $T = t\ t_c$, $U_{tot} = u\frac{r_c}{t_c}$, and $P_w = p_w p_c$, the conservation equation for water (11) becomes:

$$\varphi\frac{\partial S_w}{\partial t} + \varphi S_w c_w \frac{\partial p_w}{\partial t} + \frac{1}{r}\frac{\partial}{\partial r}\left(r f_w u_{tot}\right) + \frac{1}{r}\frac{\partial}{\partial r}\left(-r D_{cap}\frac{\partial S_w}{\partial r}\right) = 0, \tag{23}$$

where we set $c_w = p_c\tilde{c}_w$ and $D_{cap} = \tilde{D}_{cap}\frac{t_c}{r_c^2}$. Similarly, we rewrite the equation for the sum of oil and water conservation (6) as follows:

$$\frac{1}{r}\frac{\partial}{\partial r}(r u_{tot}) + \varphi S_o c_o \frac{\partial p_{cap}}{\partial t} + \varphi(S_w c_w + S_o c_o)\frac{\partial p_w}{\partial t} = 0. \tag{24}$$

We use the capillary pressure $P_{cap} = P_o - P_w$ to eliminate P_o from the Darcy (9) and find:

$$U_{tot} = -\Lambda_{tot}\frac{\partial P_w}{\partial R} + \tilde{D}_{cap}\frac{\Lambda_{tot}}{\Lambda_w}\frac{\partial S_w}{\partial R}, \tag{25}$$

which yields the dimensionless expression for u_{tot}:

$$u_{tot} = -\lambda_{tot}\frac{\partial p_w}{\partial r} + D_{cap}\frac{\lambda_{tot}}{\lambda_w}\frac{\partial S_w}{\partial r}, \tag{26}$$

where we have used $\tilde{D}_{cap} = D_{cap}\frac{r_c^2}{t_c}$ and the dimensionless mobilities λ_w and λ_o:

$$\Lambda_w = \lambda_w\frac{r_c^2}{p_c t_c},\ \ \Lambda_o = \lambda_o\frac{r_c^2}{p_c t_c}. \tag{27}$$

This means that we have according to Eqs. 17 and 18:

$$\lambda_w = \frac{k}{\mu_w}\frac{p_c t_c}{r_c^2}k_{rw} = \frac{k}{\mu_w}\frac{p_c t_c}{r_c^2}k_{rw,0}\left(\frac{S_w - S_{wc}}{1 - S_{wc}}\right)^{n_w}, \tag{28}$$

$$\lambda_o = \frac{k}{\mu_o}\frac{p_c t_c}{r_c^2}k_{ro} = \frac{k}{\mu_o}\frac{p_c t_c}{r_c^2}k_{ro,0}\left(\frac{1 - S_w}{1 - S_{wc}}\right)^{n_o} \tag{29}$$

for the (dimensionless) mobilities and according to Eq. 20:

$$D_{cap} = -\frac{\lambda_w\lambda_o}{\lambda_{tot}}\frac{dp_{cap}}{dS_w},\ \ p_{cap} = p_{cb}\left(\frac{S_w - S_{wc}}{1 - S_{wc}}\right)^{\frac{-1}{\lambda}}, \tag{30}$$

Table 2 Physical constants

Hor. perm.	$k = 10^{-13}m^2$
For. thickness	$H = 30m$
Injection rate	$Q_{inj} = 100m^3/d$
Viscosity water	$\tilde{\mu}_w = 10^{-3}Pas$
Viscosity oil	$\tilde{\mu}_g = 2\cdot 10^{-3}Pas$
Porosity	$\varphi = 0.21$
Interfacial tension	$\tilde{\sigma} = 0.03$ Pa m
Well radius	$R_w = 0.05$ m

for the (dimensionless) capillary pressure, where $p_{cb} = \frac{P_{cb}}{p_c}$.

The physical constants enter our problem (32)-(41) only via some dimensionless combinations. They occur in the equations for the mobilities in the combination $\frac{k}{\mu_w}\frac{p_c t_c}{r_c^2}$; due to our choice of scales, this combination now equals 1, which means that the water and oil mobility reduce to:

$$\lambda_w = \frac{k}{\mu_w}\frac{p_c t_c}{r_c^2}k_{rw} = k_{rw},\ \ \lambda_o = \frac{\mu_w}{\mu_o}k_{ro}, \tag{31}$$

where the ratio $\frac{\mu_o}{\mu_w}$ arises due to our scaling procedure. The injection flux $\frac{Q_{inj}}{2\pi H}\frac{t_c}{r_c^2}$ from Eq. 13 also equals 1 due to our choice of scales. The only parameters left are the combinations $p_{cb} = \frac{P_{cb}}{p_c}$ and $c_w = \tilde{c}_w p_c$ and $c_o = \tilde{c}_o p_c$, which are given in Table 3.

We summarize the model for easy reference.

2.5 Summary of the governing equations

Mass conservation equation for water (23):

$$\varphi\frac{\partial S_w}{\partial t} + \varphi S_w c_w\frac{\partial p_w}{\partial t} + \frac{1}{r}\frac{\partial}{\partial r}\left(r f_w u_{tot}\right) + \frac{1}{r}\frac{\partial}{\partial r}\left(-r D_{cap}\frac{\partial S_w}{\partial r}\right) = 0, \tag{32}$$

Sum of oil and water mass conservation (24):

$$\frac{1}{r}\frac{\partial}{\partial r}(r u_{tot}) + \varphi S_o c_o\frac{\partial p_{cap}}{\partial t} + \varphi(S_w c_w + S_o c_o)\frac{\partial p_w}{\partial t} = 0. \tag{33}$$

Darcy (34):

$$u_{tot} = -\lambda_{tot}\frac{\partial p_w}{\partial r} + D_{cap}\frac{\lambda_{tot}}{\lambda_w}\frac{\partial S_w}{\partial r}. \tag{34}$$

Mobilities:

$$\lambda_w = k_{rw} = k_{rw,0}\left(\frac{S_w - S_{wc}}{1 - S_{wc}}\right)^{n_w},\ \ \lambda_o = \frac{\mu_w}{\mu_o}k_{ro} = \frac{\mu_w}{\mu_o}k_{ro,0}\left(\frac{1 - S_w}{1 - S_{wc}}\right)^{n_o}. \tag{35}$$

Capillary pressure:

$$D_{cap} = -\frac{\lambda_w\lambda_o}{\lambda_{tot}}\frac{dp_{cap}}{dS_w},\ \ p_{cap} = p_{cb}\left(\frac{S_w - S_{wc}}{1 - S_{wc}}\right)^{\frac{-1}{\lambda}},\ \ \lambda = \frac{2}{n_w - 3} \tag{36}$$

The equations (32) to (36) are valid for $t > 0$ and $r > r_w$.
Initial conditions:

$$S_w = S_{wc},\ \ \text{at } t = 0,\ r > r_w. \tag{37}$$

$$p_w = p_{w0},\ \ \text{at } t = 0,\ \ r > r_w. \tag{38}$$

Boundary conditions:

$$S_w = 1 \text{ at } r = r_w,\ t > 0 \tag{39}$$

$$r u_{tot} = 1 \text{ at } r = r_w,\ t > 0 \tag{40}$$

$$S_w \to S_{wc}\ \text{ as } r \to \infty,\ t > 0. \tag{41}$$

The dependencies are summarized in Table 4.

Table 3 Dimensionless constants

Capillary pressure	$P_{cb} = \tilde{\sigma}\sqrt{\frac{\varphi}{k}} = 4.3 \cdot 10^4 \frac{Pam}{m}$	$p_{cb} = \frac{P_{cb}}{p_c} = 0.71$
Water compressibility	$\tilde{c}_w = 4.6 \cdot 10^{-10} Pa^{-1}$	$c_w = 4.6 \cdot 10^{-10} Pa^{-1} \cdot p_c = 2.2 \cdot 10^{-5}$
Oil compressibility	$\tilde{c}_o = 2.03 \cdot 10^{-9} Pa^{-1}$	$c_o = 2.03 \cdot 10^{-9} Pa^{-1} \cdot p_c = 1.2 \cdot 10^{-4}$

3 Similarity transformation

We express (32)–(34) in terms of η using the similarity transformation $(r, t) \rightarrow (r^2/2t = \eta)$. The product (ru_{tot}) is used as a dependent variable, i.e., the product (ru_{tot}) depends on η (see Eq. 44). Physically, this product represents the flux, i.e., the flux depends on the variable η (whereas the velocity depends on (r, t)). Using this transformation, Eq. 32 yields:

$$-\varphi\eta\frac{dS_w}{d\eta} - \eta\varphi S_w c_w \frac{dp_w}{d\eta} + \frac{d}{d\eta}\left(ru_{tot} f_w\right) - \frac{d}{d\eta}\left(2\eta D_{cap}\frac{dS_w}{d\eta}\right) = 0. \tag{42}$$

Similarly, (33) becomes:

$$\frac{d}{d\eta}(ru_{tot}) - \eta\varphi S_o c_o \frac{dp_{cap}}{dS_w}\frac{dS_w}{d\eta} - \eta\varphi(S_w c_w + S_o c_o)\frac{dp_w}{d\eta} = 0. \tag{43}$$

Finally, (34) yields:

$$ru_{tot} = -2\eta\lambda_{tot}\frac{dp_w}{d\eta} + 2\eta D_{cap}\frac{\lambda_{tot}}{\lambda_w}\frac{dS_w}{d\eta}. \tag{44}$$

Note that $p_w \sim \ln\eta$ for small η, which means that the first term on the RHS of Eq. 44 yields a finite, nonzero contribution.

The boundary conditions at the injection well $r = r_w$ are mapped to $\eta = \eta_w(t)$, where:

$$\eta_w(t) = \frac{r_w^2}{2t}. \tag{45}$$

We consider a well with a radius that is much smaller than the dimensions of the outer region. Furthermore, we are interested in the intermediate time behavior. The well radius is $R_w = 0.05$ m, then the behavior of the solution for $T > 30$ min, which corresponds to $t = 0.02$, gives

$$\eta_w(t) < 0.11. \tag{46}$$

We are interested in the behavior of the solution far away from the well, i.e., $\eta \approx 5$ and therewith $\eta_w(t) \ll 5$; and therefore, we use the approximation $\eta_w(t) \approx 0$. This means that we use the following boundary conditions as an approximation:

$$ru_{tot} = \frac{Q_{inj}}{2\pi H}\frac{t_c}{r_c^2} = 1, \; S_w = 1 \text{ at } \eta = 0. \tag{47}$$

Table 4 Overview of the dependencies

Independent variables	r, t
Dependent variables	$S_w(r,t)$, $u_{tot}(r,t)$, $p_w(r,t)$
Constitutive relations	$f_w(S_w)$, $D_{cap}(S_w)$

In Section 3.2.5, we will analyze this approximation for the boundary condition quantitatively and we will see that the error is less than 1%.

The initial condition (at $t = 0$) and the boundary condition (at $r \rightarrow \infty$) for S_w are both mapped to $\eta \rightarrow \infty$, i.e.:

$$S_w \rightarrow S_{wc} \text{ as } \eta \rightarrow \infty. \tag{48}$$

The initial condition for the pressure in the compressible case is mapped to $\eta \rightarrow \infty$, i.e.:

$$p_w \rightarrow p_{w,0} \text{ as } \eta \rightarrow \infty. \tag{49}$$

We will solve problem (42)-(49) for saturation-dependent capillary diffusion in Section 3.1 and for constant capillary diffusion in Section 3.3. We focus mainly on the incompressible case where $c_o = c_w = 0$.

3.1 Summary of the self similar (in)compressible problem

Equations (42)–(44) can be rewritten as a set of four coupled nonlinear ordinary differential equations, i.e.:

$$\frac{d}{d\eta}\begin{pmatrix} S_w \\ \frac{dS_w}{d\eta} \\ ru_{tot} \\ p_w \end{pmatrix} = \begin{pmatrix} \frac{dS_w}{d\eta} \\ f_1(S_w, \frac{dS_w}{d\eta}, ru_{tot}, p_w, \eta) \\ f_2(S_w, \frac{dS_w}{d\eta}, ru_{tot}, p_w, \eta) \\ f_3(S_w, \frac{dS_w}{d\eta}, ru_{tot}, p_w, \eta) \end{pmatrix}, \tag{50}$$

where f_3 is given by Eq. 44, f_2 is given by Eq. 43 and f_1 is given by Eq. 42. Notice that Eq. 42 is converted into two first-order equations. The functions f_1, f_2, f_3 are given by the following expressions:

$$f_3 = \frac{1}{-2\eta\lambda_{tot}}\left(ru_{tot} - 2\eta D_{cap}\frac{\lambda_{tot}}{\lambda_w}\frac{dS_w}{d\eta}\right), \tag{51}$$

$$f_2 = \eta\varphi S_o c_o \frac{dp_{cap}}{dS_w}\frac{dS_w}{d\eta} + \eta\varphi(S_w c_w + S_o c_o) f_3, \tag{52}$$

$$f_1 = \frac{1}{2\eta D_{cap}}\left(-2D_{cap}\frac{dS_w}{d\eta} - 2\eta\frac{dD_{cap}}{dS_w}\left(\frac{dS_w}{d\eta}\right)^2 - \varphi\eta\frac{dS_w}{d\eta} - \varphi S_w c_w f_3 - f_w f_2 - ru_{tot}\frac{df_w}{dS_w}\frac{dS_w}{d\eta}\right). \tag{53}$$

We have two conditions at $\eta = 0$ (see Eq. 47) and two conditions at $\eta \rightarrow \infty$ (see Eqs. 48 and 49). However, our analysis is for incompressible flows (see [2] Chapters 5 and 7); this analysis is valid for $t > \varphi\mu c_{eff} r_c^2/k \approx 1s$ for

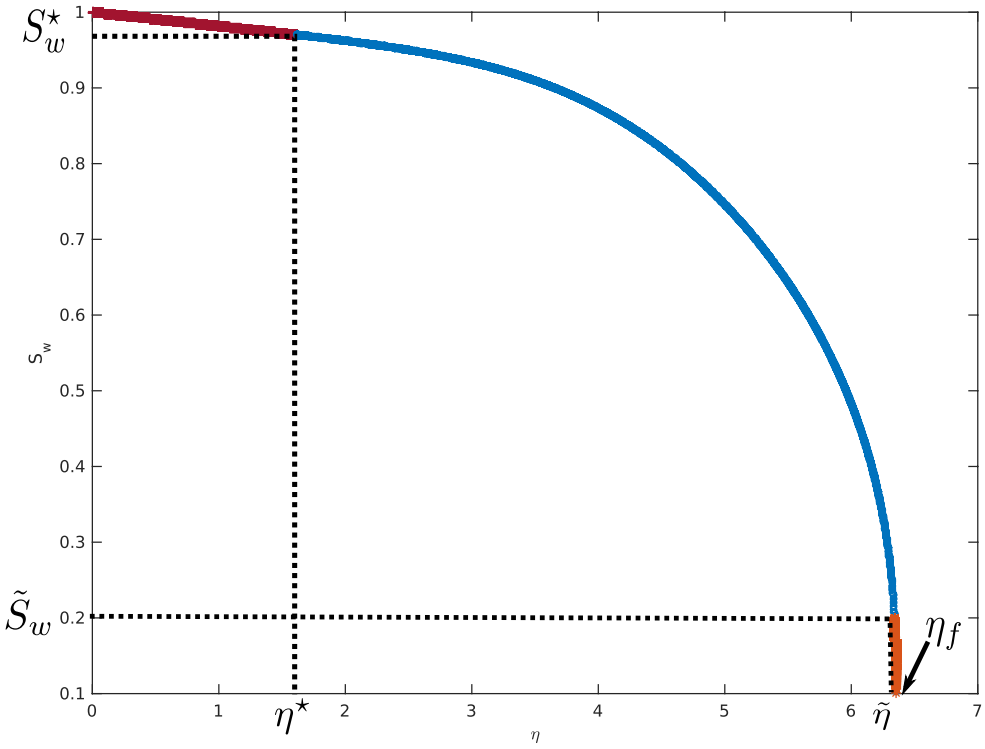

Fig. 1 Water saturation versus η. The figure shows the behavior in the region I, i.e., $0 \leq \eta \leq \eta^\star$, region II, i.e., $\eta^\star \leq \eta \leq \tilde{\eta}$, and region III, i.e., $\tilde{\eta} \leq \eta \leq \eta_f$. In region II, we use the numerical solution, whereas in regions I and III, we use an analytical approximation to solve the equations (see text)

our parameters. Therefore, compressibility effects can be disregarded for processes beyond 1 s.

3.2 Analysis in the incompressible case ($c_w = c_o = 0$)

Setting $c_w = c_o = 0$, we have $f_2 = 0$, which means that:

$$\frac{d}{d\eta}(ru_{tot}) = 0 \Rightarrow ru_{tot} = ru_{tot}(0) = 1. \tag{54}$$

Furthermore, f_1 now only depends on S_w and $\frac{dS_w}{d\eta} = S_w'$ and not on p_w. Consequently, the equation for S_w is decoupled from p_w now, which means that we can first solve the second-order ODE for S_w and use the result to find the pressure profile p_w. We do have the following problem though. Close to $S_w = 1$ and $S_w = S_{wc}$, D_{cap} becomes very small because

$$D_{cap} \sim (S_w - S_{wc})^{n_w}(S_w - S_{wc})^{\frac{1}{2}-\frac{1}{2}n_w}(1-S_w)^{n_o} = (S_w - S_{wc})^{\frac{1}{2}+\frac{1}{2}n_w}(1-S_w)^{n_o}. \tag{55}$$

This means that numerical integration close to $S_w = 1$ and $S_w = S_{wc}$ is difficult, due to the presence of D_{cap} in the denominator of f_1 (see e.g. [4], [5] for similar problems). For this reason, we split the domain in three regions (see Fig. 1):

Region I Small η and $S_w \approx 1$: $S_w^\star \leq S_w \leq 1$ and $0 \leq \eta \leq \eta^\star$

Region II Intermediate η and S_w: $\tilde{S}_w \leq S_w \leq S_w^\star$ and $\eta^\star \leq \eta \leq \tilde{\eta}$

Region III η around η_f and $S_w \approx S_{wc}$: $S_{wc} \leq S_w \leq \tilde{S}_w$ and $\tilde{\eta} \leq \eta \leq \eta_f$

Here, $\eta = \eta_f$ is the endpoint of the region where $S_w > S_{wc}$, i.e., $S_w(\eta_f) = S_{wc}$ and for $\eta \geq \eta_f$ we have $S_w = S_{wc}$ [2].

The parameters $S_w^\star$ and $\tilde{S}_w$ are numerical parameters that are chosen as close to $S_w = 1$ and $S_w = S_{wc}$ as possible; several consecutive values are chosen until no visible difference between the corresponding solutions of the model equations is observed. Once the parameters $S_w^\star$ and $\tilde{S}_w$ are fixed, all the other parameters ($\eta^\star$, $\tilde{\eta}$, η_f) follow as part of our solution to the model equations.

We will solve our problem analytically in regions I and III and we will use numerical integration in Region II as discussed in more detail in the following Sections 3.2.1–3.2.3.

3.2.1 Small η and $S_w \approx 1$: $S_w^\star \leq S_w \leq 1$

First, we choose a value $S_w^\star$ close to one; we will investigate the influence of this (numerical) choice later. We then use a linear approximation for our solution:

$$S_w(\eta) = S_w^\star + S_w'^\star(\eta - \eta^\star), \tag{56}$$

where the condition $S_w(0) = 1$ fixes $\eta^\star$ in terms of $S_w'^\star$:

$$1 = S_w(0) = S_w^\star - \eta^\star \cdot S_w'^\star \Rightarrow \eta^\star = \frac{1 - S_w^\star}{-S_w'^\star} \tag{57}$$

[2] Note that η_f truncates the domain. This is a consequence of the solution of our problem and not an a priori imposed condition.

The value of $S_w'^\star$ is determined as follows: a value of $S_w'^\star$ is picked and adjusted such that the total mass is conserved in the entire domain.

3.2.2 Intermediate η, $S_w^\star \geq S_w \geq \tilde{S}_w$

We integrate numerically from $\eta = \eta^\star$, where we have $S_w = S_w^\star$ and $S_w' = S_w'^\star$ until $\eta = \tilde{\eta}$, where $\tilde{\eta}$ is chosen such that S_w at $\tilde{\eta}$ is close to S_{wc}. We will investigate the influence of this (numerical) choice later.

3.2.3 Large $\eta \approx \eta_f$ and $S_w \approx S_{wc}$: $\tilde{S}_w \geq S_w \geq S_{wc}$

Around the toe, $\eta = \eta_f$, we have $S_w \approx S_{wc}$ and consequently the oil mobility $\lambda_o \approx 0$. This means that we have:

$$\lambda_w \sim (S_w - S_{wc})^{n_w}, \;\; D_{cap} \sim (S_w - S_{wc})^{\frac{1}{2}+\frac{1}{2}n_w}. \tag{58}$$

We assume power law behavior of S_w around η_f

$$S_w \sim S_{wc} + (\eta_f - \eta)^p, \tag{59}$$

where the exponent p remains to be determined.

Substitution of Ansatz (59) into Eq. 42 and balancing different powers of $S_w - S_{wc}$, we find (see Appendix C):

$$S_w = S_{wc} + K_1(\eta_f - \eta)^p, \;\; p = \frac{2}{n_w + 1} = 0.4, \tag{60}$$

where K_1 and η_f are constant.

This means that S_w connects continuously to the initial state $S_w = S_{wc}$ at $\eta = \eta_f$ (i.e., no shock). The derivatives of S_w though do blow up near the toe.

The constants K_1 and η_f are determined by matching the analytical solution in region III to the numerical solution in region II at $\eta = \tilde{\eta}$.

3.2.4 Global mass conservation

The unknown parameter $S_w'^\star$ has to be chosen such that we select the correct saturation profile, i.e., such that mass is globally conserved. The total amount of mass injected until time T, m_{in} equals:

$$m_{in} = Q_{inj}\rho_w T, \tag{61}$$

the mass initially present m_0 equals:

$$m_0 = \varphi \iiint_W S_{wc}\rho_w \, dV, \;\; W = [R_w, \infty) \times [0, 2\pi] \times [0, H] \tag{62}$$

and the mass present at time T, m_T equals:

$$m_T = \varphi \iiint_W S_w \rho_w \, dV. \tag{63}$$

Due to conservation of mass, we have $m_T = m_0 + m_{in}$, i.e.:

$$\varphi \iiint_W S_w \rho_w \, dV = \varphi \iiint_W S_{wc}\rho_w \, dV + Q_{inj}\rho_w T. \tag{64}$$

Using cylindrical coordinates for the triple integrals, we have:

$$2\pi H \varphi \int_{R_w}^{\infty} (S_w - S_{wc})\rho_w \; R \, dR = Q_{inj}\rho_w T. \tag{65}$$

In the incompressible case, we have constant water density; furthermore, we use $R = r\, r_c$ and $T = t\, t_c$ to obtain:

$$\varphi \int_{r_w}^{\infty} (S_w - S_{wc}) \; r \; dr = \frac{Q_{inj}}{2\pi H} \frac{t_c}{r_c^2} t. \tag{66}$$

Using $\eta = \frac{r^2}{2t} \Rightarrow d\eta = \frac{r}{t} dr$, we find:

$$\varphi \int_0^{\infty} (S_w - S_{wc}) \; d\eta = \frac{Q_{inj}}{2\pi H} \frac{t_c}{r_c^2}. \tag{67}$$

Due to our choice of scales, we have $\frac{Q_{inj}}{2\pi H} \frac{t_c}{r_c^2} = 1$; furthermore, we have $S_w = S_{wc}$ for $\eta \geq \eta_f$, which means that Eq. 67 reduces to:

$$\varphi \int_0^{\eta_f} (S_w - S_{wc}) \; d\eta = 1. \tag{68}$$

The value of $S_w'^\star$ is adjusted until (68) is satisfied.

3.2.5 Saturation-dependent capillary diffusion results

Figure 2 shows the influence of the choice of $S_w^\star$ on the results. For the scale used to display the figure, we observe that the solution with $S_w^\star = 0.95$ slightly deviates from the other three curves, which appear (almost) completely on top of each other. This means that our solution $S_w(\eta)$ is practically independent of our choice of $S_w^\star$ if $S_w^\star$ is chosen large enough, i.c., above 0.97.

Note furthermore that for $\eta < 0.11$, we have $S_w > 0.99$, which means that the error on the boundary condition due to approximating $\eta_w(t)$ by zero is in the worst case 1%.

In Fig. 3, we explore the effect of different bubbling pressures P_{cb} on the saturation profile. For small values the curves approach a steep shock-like behavior. For larger values of the bubbling pressure, which acts as a parameter for enhanced capillary diffusion, the saturation profiles are broadened. In the limit of zero capillary pressure, we find the Buckley-Leverett solution as shown in Fig. 4, which also shows that capillary diffusion broadens the front.

Figure 5 shows the water pressure profile. Our solution is only valid for $t \geq 2 \cdot 10^{-2}$ as discussed in Section 3. This occurs frequently in the case of well testing, where the very early data are ignored (see Dake [2], chapter VII, p 159 ff).

In this period, the total pressure increase of $\Delta p \approx 14$, $\Delta P = \Delta p p_c \approx 8.5$ bar is limited due to the practical duration of the test.

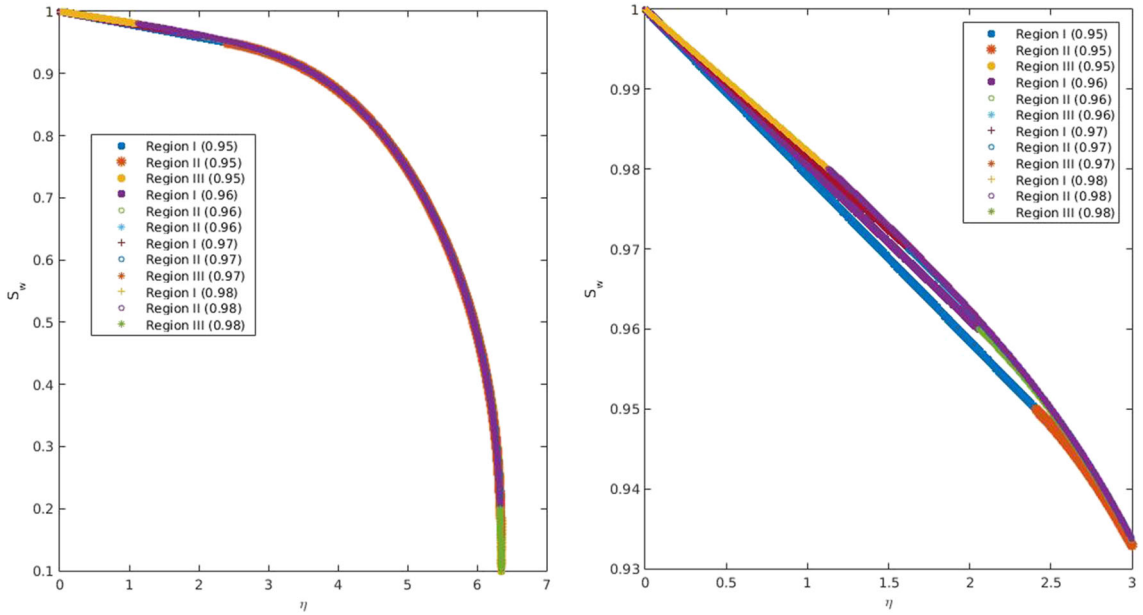

Fig. 2 Effect of the choice of $S_w^\star$ on the solution for S_w in the entire domain. The left figure shows that the dependence on $S_w^\star$ for $S_w^\star = 0.95, 0.96, 0.97, 0.98$ is negligible, but zooming in for small values of η shows that small differences can be observed for $S_w^\star = 0.95$ and $S_w^\star = 0.96$, but in practice no discernible differences for $S_w^\star \geq 0.97$. Therefore, we use $S_w^\star = 0.97$ in our computations

3.3 Constant small capillary diffusion: matched asymptotic expansions

In general, the capillary diffusion is saturation dependent, i.e.:

$$D_{cap} = -f_w \lambda_0 \frac{dp_{cap}}{dS_w}. \tag{69}$$

However, in this section, we will assume a constant (small) capillary diffusion coefficient; we will take a few representative values for D_{cap} and compute the corresponding saturation profiles. These saturation profiles are compared with the profiles (with a saturation-dependent capillary diffusion) obtained in Section 3.2.5.

We take incompressible conditions for water and oil, i.e., $c_o = c_w = 0$. This means that Eq. 43 yields:

$$\frac{d}{d\eta}(ru_{tot}) = 0 \Rightarrow ru_{tot} = \frac{Q_{inj}}{2\pi H}\frac{t_c}{r_c^2} = 1. \tag{70}$$

Furthermore, we set $D_{cap} = \varepsilon$ constant; Eq. 42 yields:

$$-\varphi\eta\frac{dS_w}{d\eta} + ru_{tot}\frac{df_w}{d\eta} - \varepsilon\frac{d}{d\eta}\left(2\eta\frac{dS_w}{d\eta}\right) = 0 \tag{71}$$

with boundary conditions

$$S_w(0) = 1, \;\; S_w(\eta_f) = S_{wc}, \tag{72}$$

where $\eta_f \approx \eta_s$ (the location of the shock in the unperturbed profile).

We will use the method of matched asymptotic expansions to obtain an approximation to the solution of Eq. 71. We solve the outer problem to obtain $S_w^{out}(\eta)$ in Section 3.3.1 and we solve the inner problem to obtain $S_w^{in}(\xi = \frac{\eta_f - \eta}{\varepsilon})$ in Section 3.3.2. The total solution of Eq. 71 is then given by:

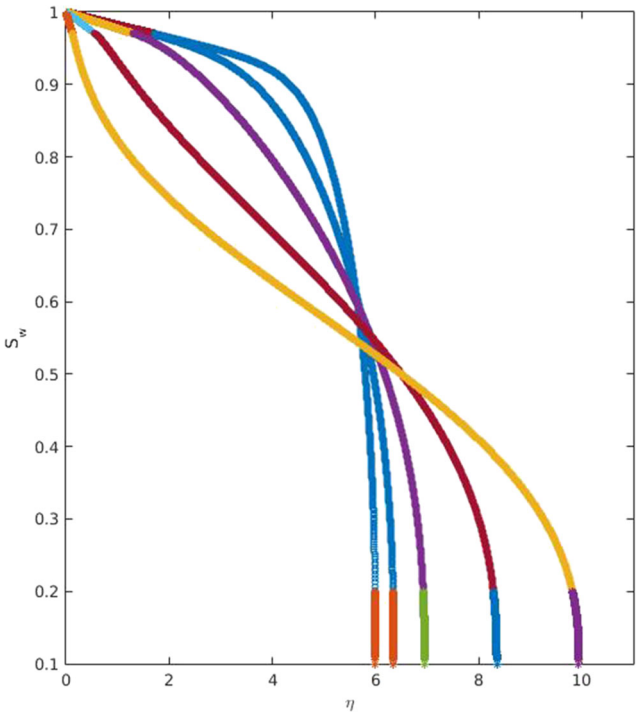

Fig. 3 Dependence of $S_w(\eta)$, for $S_w^\star = 0.97$ for different values of the bubbling pressure P_{cb}. We use P_{cb}: 5, 10,20, 50, and 100 times the bases case value of $4.3 \times 10^4 \; Pa$. The sharpest profile corresponds to $P_{cb} = 5$ times the base value. For larger values of P_{cb}, the front gets more disperse and the whole profile gets broader

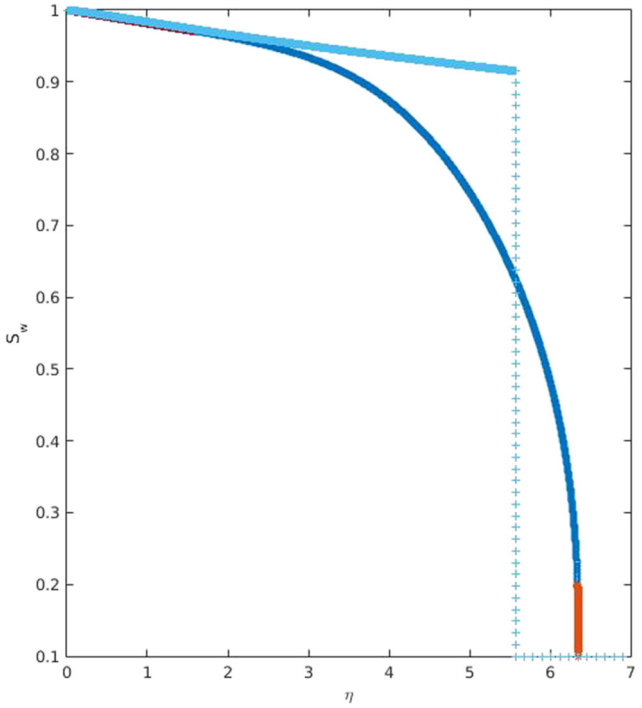

Fig. 4 Comparison of the saturation profile $S_w(\eta)$ for $S_w^\star = 0.97$ to the Buckley-Leverett solution. We observe that the overall mass balance is satisfied

$$S_w(\eta) = S_w^{out}(\eta) + S_w^{in}(\frac{\eta_f - \eta}{\varepsilon}) - S_w^m, \tag{73}$$

where the matching condition states that the inner limit of the outer solution = the outer limit of the inner solution ([13]). The matching condition

$$\lim_{\varepsilon \to 0^-} S_w^{out} = \lim_{\xi \to \infty} S_w^{in} = S_w^m \tag{74}$$

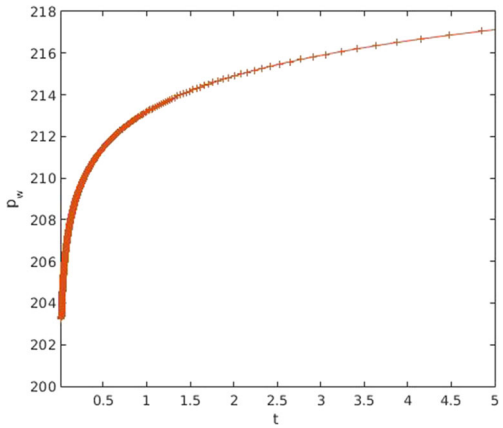

Fig. 5 Water pressure $p_w(t)$ at the inlet ($R_w = 0.1$ m) for $0.02 \leq t \leq 5$. The lower limit is chosen according to the arguments at the end of Section 3.2.5. The upper limit is taken as $t = 5$, being a reasonable limit of the duration of the test. In this period, the total pressure increase of $\Delta p \approx 14$, $\Delta P = \Delta p \cdot p_c \approx 8.5$ bar is limited due to the practical duration of the test

determines S_w^m for $\eta < \eta_s$ and the matching condition

$$\lim_{\varepsilon \to 0^+} S_w^{out} = \lim_{\xi \to -\infty} S_w^{in} = S_w^m \tag{75}$$

determines S_w^m for $\eta > \eta_s$.

3.3.1 Solution of the outer problem

In the outer problem, we neglect contributions proportional to ε, and thus Eq. 71 reduces to:

$$-\varphi\eta \frac{dS_w^{out}}{d\eta} + ru_{tot}\frac{df_w}{d\eta} = 0. \tag{76}$$

The solution of Eq. 76 is given by the Buckley-Leverett profile:

$$\eta = \frac{ru_{tot}}{\varphi}\frac{df_w}{dS_w} = \frac{1}{\varphi}\frac{df_w}{dS_w},\ 0 \leq \eta < \eta_s, \tag{77}$$

where we use that $ru_{tot} = 1$; see Eq. 70. For $\eta > \eta_s$ we have $S_w = S_{wc}$. Furthermore, the shock saturation S_w^s is obtained via Welge's tangent construction:

$$\frac{df_w}{dS_w}|_{S_w^s} = \frac{f_w(S_w^s) - f_w(S_{wc})}{S_w^s - S_{wc}} = \frac{f_w(S_w^s)}{S_w^s - S_{wc}} \Rightarrow S_w^s \approx 0.915. \tag{78}$$

Details of the derivation of Welge's tangent construction are outlined in the Appendices 1 and 2 for easy referencing for the general audience. Mathematical derivations can be found in [12] and [7].

Using Eq. (77), we obtain $\eta_s \approx 5.551$. Later on, we need η_f for which we use mass conservation. Notice, indeed that we have:

$$\int_0^{\eta_s} (S_w^{out} - S_{wc})\, d\eta = 1 \tag{79}$$

due to mass conservation; see Eq. 68.

3.3.2 Solution of the inner problem

The shock at $\eta = \eta_s$ is spread out and replaced by a front in the inner region $[\eta_s - \delta, \eta_s + \delta = \eta_f]$, where δ is $O(\varepsilon)$ small. For the inner problem, we define the new variable ξ, i.e.:

$$\xi = \frac{1}{\varepsilon}(\eta_f - \eta) \Rightarrow \eta = \eta_f - \varepsilon\xi, \tag{80}$$

which yields the following inner problem (to lowest order in ε):

$$\varphi\eta_s \frac{dS_w^{in}}{d\xi} - ru_{tot}\frac{df_w}{d\xi} - 2\eta_s \frac{d^2 S_w^{in}}{d\xi^2} = 0,\ S_w^{in}(\xi = 0) = S_{wc}, \tag{81}$$

where we used $\eta = \eta_s + O(\varepsilon)$ in the inner region. We have an additional boundary condition due to the matching

condition:

$$\lim_{\xi\to\infty} S_w^{in} = \lim_{\varepsilon\to 0^-} S_w^{out} = S_w^s. \tag{82}$$

Furthermore, we have the trivial condition:

$$\lim_{\xi\to-\infty} S_w^{in} = \lim_{\varepsilon\to 0^+} S_w^{out} = S_{wc}. \tag{83}$$

This means that our total solution (outer solution plus inner solution minus matching saturation) becomes:

$$S_w = \begin{cases} S_w^{out}(\eta) + S_w^{in}(\frac{\eta_f-\eta}{\varepsilon}) - S_w^s & 0 \le \eta \le \eta_s \\ S_w^{in}(\frac{\eta_f-\eta}{\varepsilon}) & \eta_s < \eta < \eta_f \\ S_{wc} & \eta \ge \eta_f \end{cases} \tag{84}$$

because $S_w^{out} = S_{wc} = S_w^m$ (see Eq. 83) for $\eta > \eta_s$.

Integrating (81) once yields:

$$\varphi\eta_s S_w^{in} - r u_{tot} f_w - 2\eta_s \frac{dS_w^{in}}{d\xi} = \varphi\eta_s S_{wc} - 2\eta_s \frac{dS_w^{in}}{d\xi}|_{S_{sc}}, \tag{85}$$

i.e.,

$$\frac{dS_w^{in}}{d\xi} = f_w \frac{r u_{tot}}{-2\eta_s} + \frac{1}{2}\varphi S_w^{in} - \frac{1}{2}\varphi S_{wc} + \frac{dS_w^{in}}{d\xi}|_{S_{wc}} = g(S_w^{in}) + K, \tag{86}$$

where we set the constant $K = \frac{dS_w^{in}}{d\xi}|_{S_{sc}}$ and

$$g(S_w^{in}) = f_w \frac{r u_{tot}}{-2\eta_s} + \frac{1}{2}\varphi S_w^{in} - \frac{1}{2}\varphi S_{wc}. \tag{87}$$

We use separation of variables to solve (86) and find

$$\xi = \int_{u=S_{wc}}^{S_w^{in}} \frac{1}{g(u)+K} du. \tag{88}$$

We use the matching condition (82) to determine the constant K. The integral:

$$\int_{u=S_{wc}}^{S_w^s} \frac{1}{g(u)+K} du \tag{89}$$

has to diverge due to the matching condition (82); $\xi = \infty$ if and only if $S_w^{in} = S_w^s$. Note that the integration interval is finite and that $g(u)$ is continuous; the integral only blows up if the denominator equals 0, i.e., if $g(u)+K = 0$. Notice that we have $g(S_w^s) = 0$; this means that we need $K = 0$ in order to have a divergent integral around $S_w = S_w^s$, i.e.:

$$\xi = \int_{u=S_{wc}}^{S_w^{in}} \frac{1}{g(u)} du. \tag{90}$$

Equation (90) is integrated numerically to obtain $\xi(S_w^{in})$ and inverted to obtain $S_w^{in}(\xi)$.

3.3.3 Determining η_f to first order in ε

We use global mass conservation to compute the width of the front and thus η_f. According to Eq. 68, we have:

$$\varphi \int_0^{\eta_f} (S_w - S_{wc})\, d\eta = 1, \tag{91}$$

and therefore using Eq. 84 we find:

$$\varphi \int_0^{\eta_s} (S_w^{out} + S_w^{in} - S_w^s - S_{wc})\, d\eta + \varphi \int_{\eta_s}^{\eta_f} (S_w^{in} - S_{wc})\, d\eta = 1, \tag{92}$$

which yields (using Eq. 79, part of the first integral equals 1, and therefore the RHS becomes 0).

$$\varphi \int_0^{\eta_s} (S_w^{in} - S_w^s)\, d\eta + \varphi \int_{\eta_s}^{\eta_f} (S_w^{in} - S_{wc})\, d\eta = 0. \tag{93}$$

Equation (93) can be rewritten as:

$$\int_0^{\eta_s} (S_w^{in} - S_{wc})\, d\eta - \int_0^{\eta_s} (S_w^s - S_{wc})\, d\eta + \int_{\eta_s}^{\eta_f} (S_w^{in} - S_{wc})\, d\eta = 0 \tag{94}$$

and combining the first and the last integral and computing the second we find that:

$$\int_0^{\eta_f} (S_w^{in} - S_{wc})\, d\eta = \eta_s (S_w^s - S_{wc}). \tag{95}$$

Setting $\eta = \eta_f - \varepsilon\xi$ yields:

$$\varepsilon \int_0^{\frac{\eta_f}{\varepsilon}} (S_w^{in} - S_{wc})\, d\xi = \eta_s (S_w^s - S_{wc}). \tag{96}$$

The product of ε and the integral on the LHS will be finite; numerically, we compute the integral first, and then we multiply by ε. For small values of ε, this might cause numerical problems. We circumvent those problems by splitting the integral into two parts. For large values of ξ ($\xi > \delta$, where δ is specified below), the integrand is approximately constant and equal to $S_w^s - S_{wc}$ because we have $\lim_{\xi\to\infty} S_w^{in}(\xi) = S_w^s$ due to our matching condition (82).

We use Eq. 90 to compute δ such that $S_w^s - S_w^{in} < 10^{-3}$ for $\xi > \delta$. We then approximate S_w^{in} by S_w^s in the integrand of Eq. 96 for $\delta < \xi < \frac{\eta_f}{\varepsilon}$ and we split the integral from Eq. 96 in two parts as follows:

$$\begin{aligned} \varepsilon \int_0^{\frac{\eta_f}{\varepsilon}} (S_w^{in} - S_{wc})\, d\xi &= \varepsilon \int_0^{\delta} (S_w^{in} - S_{wc})\, d\xi + \varepsilon \int_{\delta}^{\frac{\eta_f}{\varepsilon}} (S_w^s - S_{wc})\, d\xi \\ &= \varepsilon \int_0^{\delta} (S_w^{in} - S_{wc})\, d\xi + (\eta_f - \delta\varepsilon)(S_w^s - S_{wc}). \end{aligned} \tag{97}$$

We substitute this expression in Eq. 96 and we solve for the end point of the saturation profile η_f ($S_w = S_{wc}$ for $\eta > \eta_f$) to obtain:

$$\eta_f = \eta_s + \delta\varepsilon - \frac{\varepsilon}{S_w^s - S_{wc}} \int_0^{\delta} (S_w^{in} - S_{wc})\, d\xi. \tag{98}$$

Note that the parameter δ is order 1. This is so because we stay away far enough from $g(u) = 0$, i.e., $u = S_w^s$ in Eq. 90. Furthermore, notice that the product $\delta\varepsilon$ is a measure of the

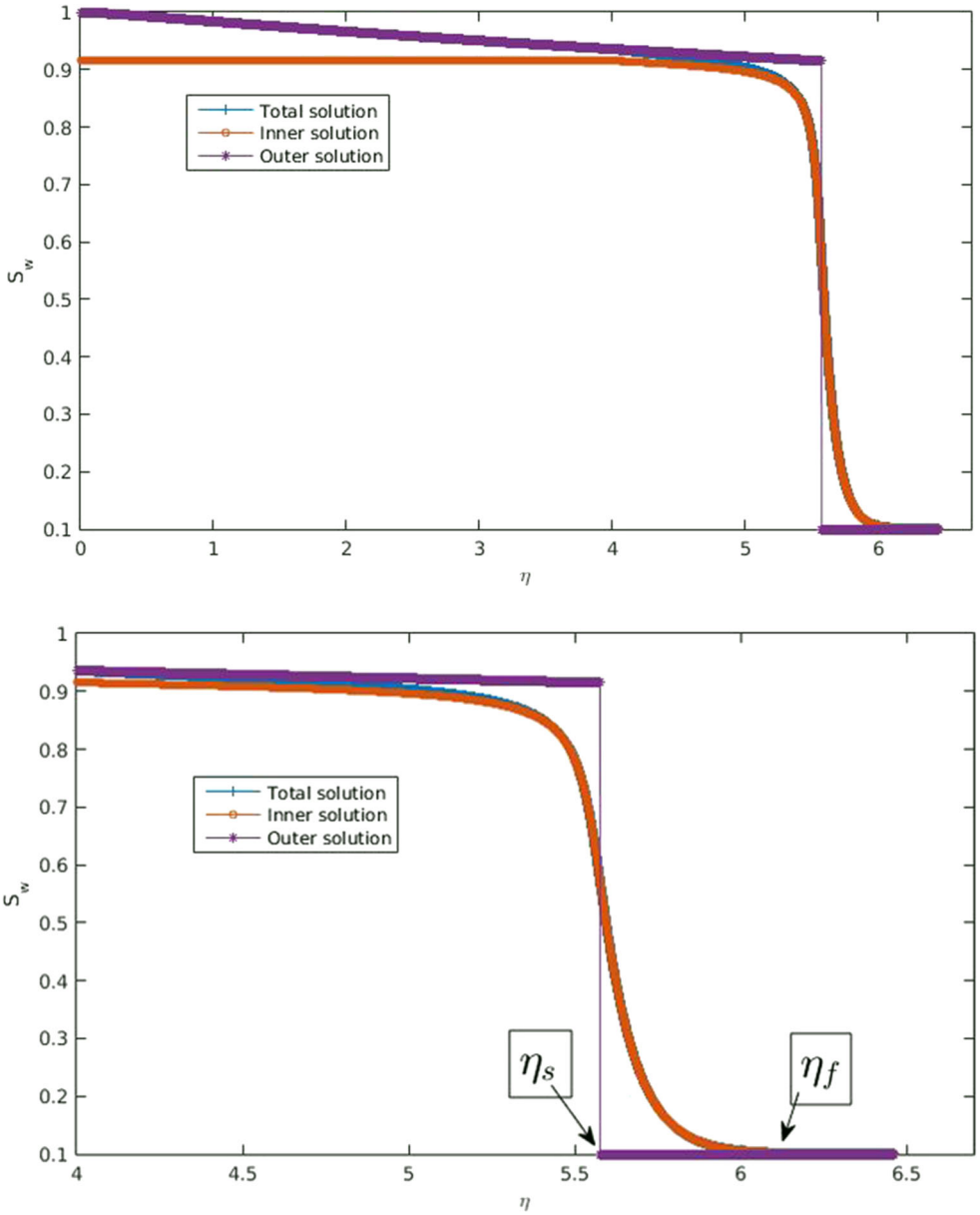

Fig. 6 Inner, outer and total solution of the saturation profile for $\varepsilon = 10^{-2}$. Consecutively the solution over the entire η range, and a zoom in the front region are given. At $\eta \approx 4.8$ the transition from the outer to the inner solution occurs

width of the front, which is approximately given by $\eta_f - \eta_s$ (see Fig. 6).

3.3.4 Numerical and analytical results

Figures 6, 7, and 8 give the results of the matched asymptotic expansions, for two values of ε. For larger values of ε, we obtain a dispersed front and for very small values of ε we approach the Buckley-Leverett solution.

4 Numerical results

We consider a fully coupled, implicit numerical solution approach based on finite elements, which is solved with the mathematical module of COMSOL to solve the model equations in weak form. We consider the spatial domain $0 \leq x \leq L$ of length $L = 100$m, where the Dirichlet boundary condition is taken at the production side, $x = L$. The grid size in the numerical simulation is 0.001 m, which corresponds to a spatial resolution of 100,000. This is fine enough to resolve the salient features. The reservoir parameters are given in Tables 2 and 3.

Numerical results for the base case are shown in Fig. 9. Here, the numerical simulation confirms the mentioned analytical results. As shown in Fig. 9, for smaller capillary diffusion (lower P_{cb}), the front is steep, whereas for higher capillary diffusion, the front is smeared out.

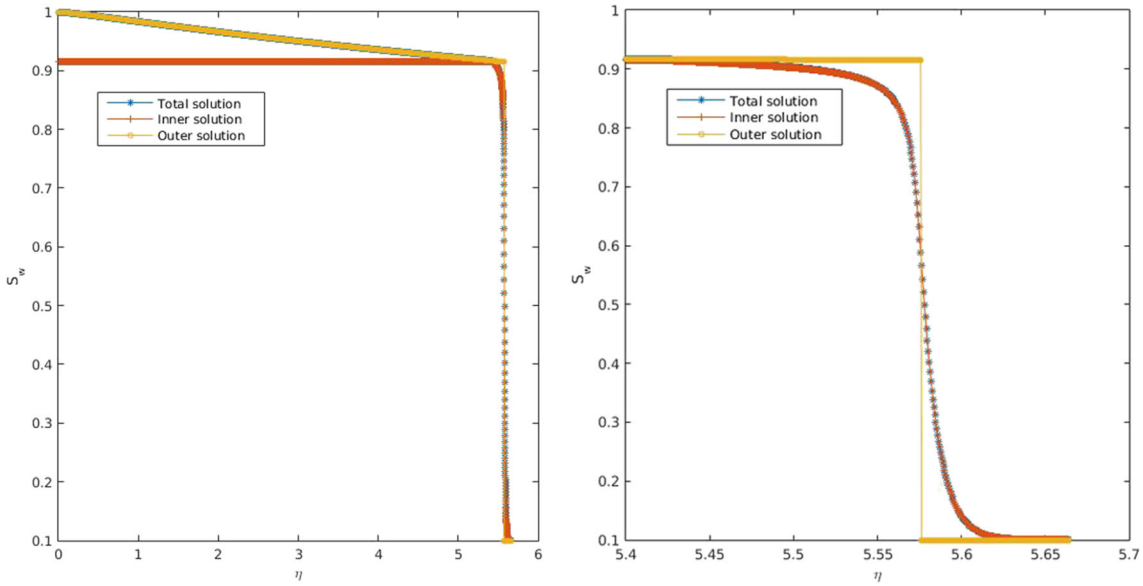

Fig. 7 Inner, outer, and total solution of the saturation profile for $\varepsilon = 10^{-3}$. On the left is the solution over the entire η range; on the right is a zoom in the front region. It is difficult to observe the transition from the inner to the outer solution due to the small value of ε

5 Discussion

Figure 10 compares the analytical and numerical solutions of problems (32)–(41). The solutions practically coincide over the entire domain except where the downstream solution connects to the initial condition.This is due to the fact that capillary diffusion vanishes at this point (toe). This causes power law behavior for the saturation S_w, i.e., S_w is a continuous function of η at the toe, but the derivatives blow up. In the analytical solution, we use an explicit expression for S_w to circumvent this problem. In the latest versions of COMSOL, numerical problems ensuing from the large values of the derivatives at the toe are suppressed by algorithms implemented in COMSOL. For smaller values of the capillary diffusion coefficient, i.e., less than five times P_{cb}, numerical problems occur at the injection point due to the vanishing capillary diffusion. Figure 11 compares the analytical solution of problems (32)–(41) with the analytical solution of problems (71)–(75), i.e., the problem with a saturation-dependent capillary diffusion to the problem with a constant diffusion

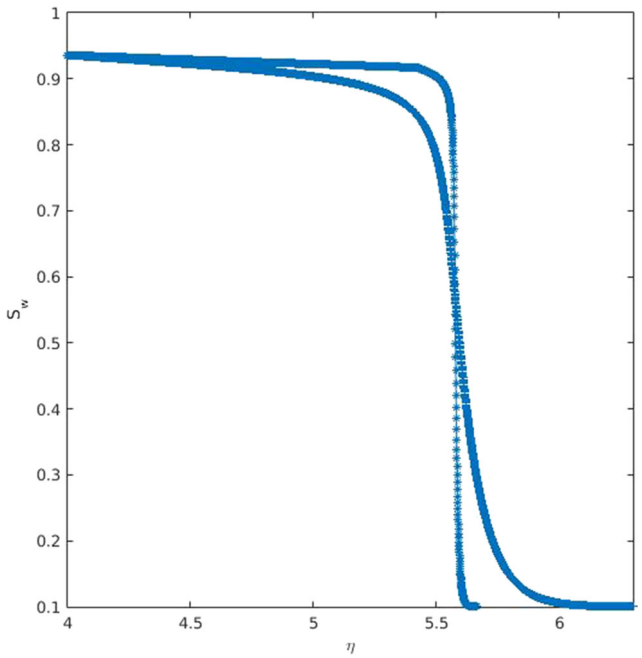

Fig. 8 Total solution of the saturation profile for $\varepsilon = 10^{-2}$ and $\varepsilon = 10^{-3}$. Large values of ε lead to a more spread out wave

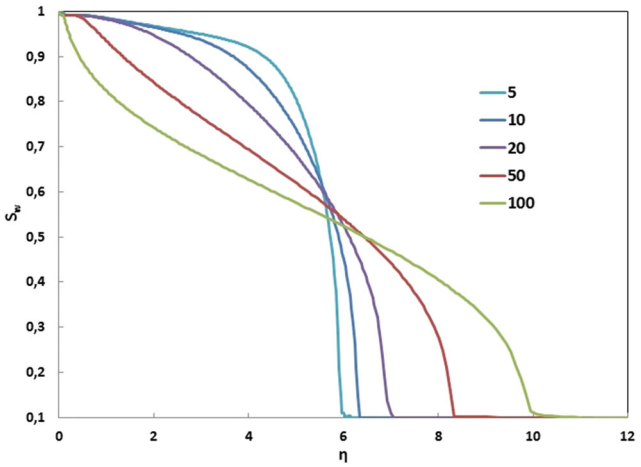

Fig. 9 The saturation profile $S_w(\eta)$ is given for different values of the bubbling pressure P_{cb}. We use P_{cb} : 5, 10,20, 50, and 100 times the bases case value of 4.3×10^4 Pa. The sharpest profile corresponds to $P_{cb} = 5$ times the base value. For larger values of P_{cb}, the front gets more disperse and the whole profile gets broader. For smaller values of P_{cb}, COMSOL is not able to find a solution

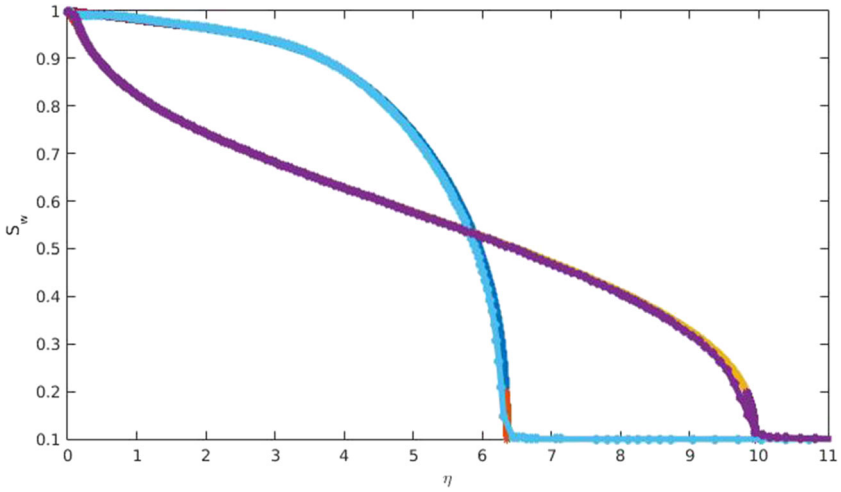

Fig. 10 Combination of Figs. 3 (saturation profile obtained by the analytical method) and 9 (saturation profile obtained using COMSOL) for P_{cb} 10 and 100 times of the base value. We observe that both methods yield the same saturation profile

coefficient of comparable magnitude. Close to the injection point, the solutions more or less coincide. Close to the toe, we observe that the problem with constant diffusion has a smooth saturation profile, whereas the solution with the saturation-dependent diffusion coefficient shows power law behavior. Note that a very small constant diffusion coefficient admits a viable solution, which can be obtained with the method of matched asymptotic expansions.

6 Conclusion

The equations for radial Buckley-Leverett flow can be reduced to a first-order ODE using a similarity coordinate $\eta = r^2/(2t)$ transformation of the model equations. The resulting ODE can be solved in a similar way as the 1D problem. The solution consists of a rarefaction wave, followed by a shock to the constant initial state. When we include capillary diffusion, we obtain the Rapoport-Leas equation, which can be reduced to a second-order ODE using the same similarity transformation. This problem can be solved with a combination of analytical and numerical techniques. In this case, we observe that the shock is replaced by a curve that shows power law behavior; the saturation profile is continuous, but the derivatives blow up at the toe. We compare the similarity solution of the second-order ODE to a numerical solution of the initial value problem over the entire domain. The solutions for the saturation profile show excellent agreement. As long as we stay away from the connate water saturation, where the capillary pressure blows up, the solutions for the water pressure also show excellent agreement. If we replace the saturation-dependent capillary diffusion by a constant diffusion coefficient, we obtain a simpler problem, which can be solved with the method of matched asymptotic expansions. In this case, the shock is replaced by a smooth profile.

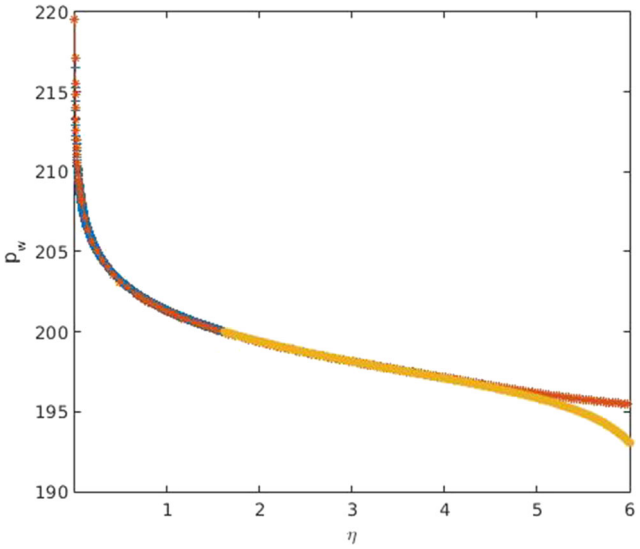

Fig. 11 Pressure p_w as function of η obtained by the analytical method and using COMSOL for P_{cb} 10 times the base value. We observe that both methods yield the same pressure profile until $\eta = 5$. Note that for $\eta > 5$, the time $t < 2 \times 10^{-3}$ at $r = r_w$, which is outside the range of validity of the analytical solution (and outside the range of interest)

Our analysis is for incompressible flows (see [2], Chapters 5 and 7). It is shown in [2] that this analysis is valid for $t > \varphi\mu c_{eff} r_c^2/k$ corresponding with our parameter values to approximately 1 s. Therefore, compressibility effects can be disregarded for processes beyond 1 s. For other parameters, e.g., for gas shales, this analysis can be used including the self-similar transformation for $t < \varphi\mu c_{eff} r_c^2/k$. This results in a system of four coupled ODEs in terms of η. In general, the similarity transformation reduces the number of independent variables from two to one; this may considerably simplify the equations used to interpret the results of this type of well test problems.

Appendix 1: Rankine-Hugoniot condition

Mass conservation across the shock specifies the shock velocity in terms of the shock saturation; this condition is called the Rankine-Hugoniot condition. In the case of radial flow, the shock velocity v_s is replaced by $\eta_s = rv_s$, where η_s can be interpreted as (2D) radial flux up to a factor of 2π.

1.1 The Rankine-Hugoniot condition in the rectilinear (1D) case

We will first give a short summary of the 1D problem. In the 1D (incompressible) problem with $p_c = 0$, we have mass conservation:

$$\varphi \frac{\partial S_w}{\partial t} + \frac{\partial u_w}{\partial x} = 0, \ \varphi \frac{\partial S_o}{\partial t} + \frac{\partial u_o}{\partial x} = 0 \tag{99}$$

and Darcy

$$u_w = -\lambda_w \frac{\partial p}{\partial x}, \ u_0 = -\lambda_o \frac{\partial p}{\partial x} \Rightarrow u_w = f_w u_{tot}, \ u_{tot} = u_w + u_o \tag{100}$$

with boundary conditions and initial condition:

$$S_w(0,t) = 1, \ u_w(0,t) = u_{inj}, \ S_w(x,0) = S_{wc}, \tag{101}$$

where u_{inj} is the constant injection velocity. Adding both (99) and using the boundary conditions (101), we find:

$$u_{tot} = u_{inj} \text{ (constant)}, \tag{102}$$

which means that our problems (99)–(100) reduces to:

$$\varphi \frac{\partial S_w}{\partial t} + u_{inj} \frac{\partial f_w}{\partial x} = 0, \ S_w(0,t) = 1, \ S_w(x,0) = S_{wc}. \tag{103}$$

Setting $\eta = \frac{x}{t}$ we find a rarefaction wave (similarity solution):

$$\eta = \frac{u_{inj}}{\varphi} \frac{df_w}{dS_w}, \ 0 \le \eta < \eta_s \tag{104}$$

followed by a shock at $\eta = \eta_s$ to the constant state $S_w = S_{wc}$. The self similar variable η can be interpreted as a velocity, i.e., saturations above the shock saturation S_w^s travel with speed $u = \frac{u_{inj}}{\varphi} \frac{df_w}{dS_w}$. The velocity of the shock v_s can be expressed in terms of the saturations in front of the shock and behind the shock using mass conservation as follows. The shock is located at position x_0 at time t_0 and moves to the right to the position $x_0 + \Delta x$ at time $t_0 + \Delta t$. This means that we have at $t = t_0 + \Delta t$:

$$S_w = S_w^+ \text{ for } x > x_0 + \Delta x \tag{105}$$

slightly in front of the shock and

$$S_w \approx S_w^- \text{ for } x \in [x_0, x_0 + \Delta x) \tag{106}$$

behind the shock (S_w is approximately constant in $[x_0, x_0 + \Delta x)$ if Δx is small enough). Furthermore, we have the (1D) volumetric velocities in front of/behind the shock:

$$u_w^+ = u_{inj} f_w(S_w^+), \ u_w^- = u_{inj} f_w(S_w^-). \tag{107}$$

We use the following mass balance in the region $[x_0, x_0 + \Delta x]$:

$$(u_w^- - u_w^+)\Delta t \approx \varphi(S_w^- - S_w^+)\Delta x, \tag{108}$$

where the net inflow is given by the LHS and the mass accumulation is given on the RHS. Taking the limit $\Delta t \to 0$ yields the shock velocity:

$$v_s = \frac{u_{inj}}{\varphi} \frac{f_w(S_w^-) - f_w(S_w^+)}{S_w^- - S_w^+}. \tag{109}$$

Notice that Eq. 109 only specifies v_s (or η_s) in terms of the saturations S_w^- and S_w^+; these saturation values around the shock are given by another physical mechanism called the entropy condition, described in Section B.

1.2 The Rankine-Hugoniot condition in the radial case

The derivation of the Rankine-Hugoniot in the radial case goes along the same lines as the 1D case. In the radial (incompressible) problem, we have:

$$\varphi \frac{\partial S_w}{\partial t} + \frac{1}{r} \frac{\partial}{\partial r}(u_w r) = 0, \ \varphi \frac{\partial S_o}{\partial t} + \frac{1}{r} \frac{\partial}{\partial r}(u_o r) = 0, \tag{110}$$

and Darcy

$$u_w = -\lambda_w \frac{\partial p}{\partial r}, \ u_0 = -\lambda_o \frac{\partial p}{\partial r} \Rightarrow u_w = f_w u_{tot}, \ u_{tot} = u_w + u_o \tag{111}$$

with boundary condition and initial condition

$$S_w(0,t) = 1, \ r u_w(0,t) = 1 \ S_w(r,0) = S_{wc}. \tag{112}$$

Adding both (110) and using the boundary conditions (112), we find:

$$r u_{tot} = 1 \text{ (constant)}, \tag{113}$$

which means that our problems (110)–(111) reduce to

$$\varphi \frac{\partial S_w}{\partial t} + \frac{r u_{tot}}{r} \frac{\partial f_w}{\partial x} = 0, \;\; S_w(0,t) = 1, \;\; S_w(x,0) = S_{wc}. \tag{114}$$

(we keep the product ru_{tot} throughout the section, even though it equals 1, to facilitate comparison with the 1D-case). Setting $\eta = \frac{r^2}{2t}$, we find a rarefaction wave:

$$\eta = \frac{r u_{tot}}{\varphi} \frac{df_w}{dS_w}, \;\; 0 \leq \eta < \eta_s \tag{115}$$

followed by a shock at $\eta = \eta_s$ to the constant state $S_w = S_{wc}$. The self similar variable η can be interpreted as 2D-volumetric flux ($\eta = ru$), i.e., saturations above S_w^s travel with "speed" $ru = \frac{ru_{tot}}{\varphi} \frac{df_w}{dS_w}$.

The shock is located at position r_0 at time t_0 and at position $r_0 + \Delta r$ at time $t_0 + \Delta t$. This means that we have

$$S_w = S_w^+ \text{ for } r > r_0 + \Delta r \tag{116}$$

slightly in front of the shock and

$$S_w \approx S_w^- \text{ for } r \in [r_0, r_0 + \Delta r) \tag{117}$$

behind the shock (S_w is approximately constant in $[r_0, r_0 + \Delta r)$ if Δr is small enough). Furthermore, we have the (2D) volumetric velocities in front of/behind the shock:

$$ru_w^+ = r u_{tot} f_w(S_w^+), \;\; ru_w^- = r u_{tot} f_w(S_w^-). \tag{118}$$

The mass balance (net inflow equals mass accumulation) in the annulus between $r = r_0$ and $r = r_0 + \Delta r$ yields:

$$2\pi r(u_w^- - u_w^+)\Delta t \approx \varphi 2\pi r (S_w^- - S_w^+)\Delta r. \tag{119}$$

Taking the limit $\Delta t \to 0$ yields the shock velocity:

$$r v_s = \frac{r u_{tot}}{\varphi} \frac{f_w(S_w^-) - f_w(S_w^+)}{S_w^- - S_w^+}. \tag{120}$$

Notice that Eq. 120 only specifies v_s (or $\eta_s = r v_s$) in terms of the saturations S_w^- and S_w^+; these saturation values are given by the entropy condition in Section 2.

Appendix 2: The entropy condition

The Rankine-Hugoniot condition does not specify the shock saturation. Behind the shock, the velocity (in the 1D case) is given as:

$$u = \frac{u_{tot}}{\varphi} \frac{df_w}{dS_w}. \tag{121}$$

This means that we have at the shock saturation $S_w^s = S_w^-$

$$v_s \geq \left. \frac{u_{tot}}{\varphi} \frac{df_w}{dS_w} \right|_{S_w^s}. \tag{122}$$

If $v_s < \left. \frac{u_{tot}}{\varphi} \frac{df_w}{S_w} \right|_{S_w^s}$ higher saturations would overtake the shock and the solution would become multivalued. According to the entropy condition (140) derived in Section 2.1 we also have:

$$v_s \leq \left. \frac{u_{tot}}{\varphi} \frac{df_w}{dS_w} \right|_{S_w^s}, \tag{123}$$

which means that we have:

$$v_s = \left. \frac{u_{tot}}{\varphi} \frac{df_w}{dS_w} \right|_{S_w^s}, \tag{124}$$

i.e.,

$$\frac{f_w(S_w^s) - f_w(S_w^+)}{S_w^s - S_w^+} = \left. \frac{df_w}{dS_w} \right|_{S_w^s}. \tag{125}$$

Due to the specific functional form of f_w there is usually one solution that shocks to the base state, which means that $S_w^+ = S_{wc}$, i.e.,

$$\frac{f_w(S_w^s) - f_w(S_{wc})}{S_w^s - S_{wc}} = \left. \frac{df_w}{dS_w} \right|_{S_w^s}. \tag{126}$$

This means that Eq. 126 has only one solution S_w^s, which corresponds to the solution found using Welge's tangent construction.

In the radial case, a similar argument holds; we need:

$$r v_s \geq \left. \frac{r u_{tot}}{\varphi} \frac{df_w}{dS_w} \right|_{S_w^s}, \tag{127}$$

otherwise higher saturations would have a higher 2D volumetric velocity and would overtake the shock, leading to a multivalued solution. Furthermore, we will show in Section 2.2 (see Eq. 143) that:

$$r v_s = \eta_s \leq \left. \frac{r u_{tot}}{\varphi} \frac{df_w}{dS_w} \right|_{S_w^s} \tag{128}$$

and we can conclude that the shock saturation is given by:

$$r v_s = \left. \frac{r u_{tot}}{\varphi} \frac{df_w}{dS_w} \right|_{S_w^s} \Rightarrow \frac{f_w(S_w^s) - f_w(S_{wc})}{S_w^s - S_{wc}} = \left. \frac{df_w}{dS_w} \right|_{S_w^s}, \tag{129}$$

just as in the 1D case.

2.1 The entropy condition in the 1D case

The idea of the entropy condition is that the physical solution of problems (99)–(101) is given by the solution of equation:

$$\varphi \frac{\partial S_w}{\partial t} + \frac{\partial u_w}{\partial x} = \epsilon \frac{\partial^2 S_w}{\partial x^2}, \;\; u_w = u_{tot} f_w(S_w), \tag{130}$$

with boundary condition and initial condition

$$S_w(0,t) = 1, \;\; S_w(x,0) = S_{wc} \tag{131}$$

in the limit $\epsilon \to 0$.

We can solve problems (130)–(131) using the method of matched asymptotic expansions around the shock. The outer

solution is given by a rarefaction wave, possibly followed by a constant state, i.e., approaching the shock we find:

$$\lim_{\eta\to 0^-} S_w^{out} = S_w^s, \tag{132}$$

where we use the moving coordinate $\eta = x - v_s t$. We solve the inner problem in the comoving frame and we set:

$$\xi = \frac{x - v_s t}{\epsilon} \tag{133}$$

to obtain the inner problem:

$$-\varphi v_s \frac{dS_w^{in}}{d\xi} + u_{inj}\frac{df_w}{d\xi} = \frac{d^2 S_w^{in}}{d\xi^2},\ S_w^{in}(\xi = 0) = S_{wc},\ \lim_{\xi\to-\infty} S_w^{in} = S_w^s. \tag{134}$$

Integrating once from $-\infty$ to ξ yields:

$$-\varphi v_s S_w^{in} + u_{inj} f_w = \frac{dS_w^{in}}{d\xi} - \varphi v_s S_w^s + u_{tot} f_w(S_w^s), \tag{135}$$

where we used that $\frac{dS_w^{in}}{d\xi}|_{S_w^s} \to 0$ as $\xi \to -\infty$[3]. Solving for $\frac{dS_w^{in}}{d\xi}$ yields:

$$\frac{dS_w^{in}}{d\xi} = u_{inj}\left(f_w - f_w(S_w^s)\right) - \varphi\left(S_w^{in} - S_w^s\right) \tag{136}$$

and using a Taylor approximation for f_w around S_w^s we obtain:

$$\frac{dS_w^{in}}{d\xi} = u_{inj}\left.\frac{df_w}{dS_w}\right|_{S_w^s}(S_w^{in} - S_w^s) - \varphi v_s\left(S_w^{in} - S_w^s\right), \tag{137}$$

i.e.,

$$\frac{dS_w^{in}}{d\xi} = \left(u_{inj}\left.\frac{df_w}{dS_w}\right|_{S_w^s} - \varphi v_s\right)\left(S_w^{in} - S_w^s\right) \le 0, \tag{138}$$

where the inequality holds because S_w^{in} is a decreasing function of ξ; $\frac{dS_w^{in}}{d\xi}$ is determined by S_w^{in} (see Eq. 136), so if $\frac{dS_w^{in}}{d\xi}$ would be positive for some value of S_w^{in}, the saturation will never drop below this value of S_w^{in} and reach S_{wc}. We have $S_w^{in} - S_w^s \le 0$ which means that we need:

$$u_{inj}\left.\frac{df_w}{dS_w}\right|_{S_w^s} - \varphi v_s \ge 0, \tag{139}$$

which leads to the following inequality for v_s

$$v_s \le \frac{u_{inj}}{\varphi}\left.\frac{df_w}{dS_w}\right|_{S_w^s} \tag{140}$$

used in the previous section.

[3]The derivative approaches zero because S_w^{in} is a continuously decreasing function of ξ, approaching a constant as $\xi \to -\infty$ (see the last equation in (134))

2.2 The entropy condition in the radial case

We use the method of matched asymptotic expansions (see Section 3.3) to derive (128). Integrating (81) from ∞ to ξ yields:

$$\varphi\eta_s(S_w - S_w^s) - r u_{tot}(f_w - f_w(S_w^s)) = 2\eta_s\frac{dS_w}{d\xi}, \tag{141}$$

where we used that $\left.\frac{dS_w^{in}}{d\xi}\right|_{S_w^s} \to 0$ as $\xi \to \infty$.[4] Using a Taylor approximation for f_w around S_w^s and solving for $\frac{dS_w}{d\xi}$ we find:

$$2\eta_s\frac{dS_w}{d\xi} = \left(\varphi\eta_s - r u_{tot}\left.\frac{df_w}{dS_w}\right|_{S_w^s}\right)\left(S_w - S_w^s\right). \tag{142}$$

Notice that the LHS of Eq. 142 is positive (the saturation is an increasing function of ξ due to the choice of ξ), which means that we find:

$$\varphi\eta_s - r u_{tot}\left.\frac{df_w}{dS_w}\right|_{S_w^s} \le 0 \Rightarrow \eta_s \le \frac{r u_{tot}}{\varphi}\left.\frac{df_w}{dS_w}\right|_{S_w^s}. \tag{143}$$

Appendix 3: Mathematical details of Section 3.2.3

In this section, we will discuss briefly how Eq. 60 is derived using Eqs. 58 and 59.

For $S_w \approx S_{wc}$, only the first and last terms of Eq. 42 are nonzero. The second term vanishes due to the incompressibility assumption; for the third term, we have:

$$\frac{d}{d\eta}(r u_{tot} f_w) = \frac{df_w}{d\eta}, \tag{144}$$

because $r u_{tot} = 1$ in the incompressible case (see Eq. 54). Furthermore, we have $\lambda_o \approx 0 \Rightarrow f_w \approx 1$, which means that the third term indeed vanishes.

This means that we have to balance the first and fourth terms to get a nontrivial solution.

For the first term $-\varphi\eta\frac{dS_w}{d\eta}$, we find:

$$-\varphi\eta\frac{dS_w}{d\eta} \sim -\varphi\eta_f p(\eta_f - \eta)^{p-1} \tag{145}$$

and for the fourth term $\frac{d}{d\eta}\left(2\eta D_{cap}\frac{dS_w}{d\eta}\right)$, we find three contributions:

$$2D_{cap}\frac{dS_w}{d\eta} + 2\eta\frac{D_{cap}}{d\eta}\frac{dS_w}{d\eta} + 2\eta D_{cap}\frac{d^2 S_w}{d\eta^2}, \tag{146}$$

where

$$2D_{cap}\frac{dS_w}{d\eta} \sim (\eta_f - \eta)^{\frac{1}{2}p + \frac{1}{2}pn_w}(\eta_f - \eta)^{p-1}, \tag{147}$$

[4]The derivative approaches zero because S_w^{in} is a continuously increasing function of ξ, approaching a constant as $\xi \to \infty$ (see Eq. 74)

$$2\eta \frac{D_{cap}}{d\eta}\frac{dS_w}{d\eta} \sim (\eta_f - \eta)^{\frac{1}{2}p+\frac{1}{2}pn_w-1}(\eta_f - \eta)^{p-1} \quad (148)$$

and

$$2\eta D_{cap}\frac{d^2S_w}{d\eta^2} \sim (\eta_f - \eta)^{\frac{1}{2}p+\frac{1}{2}pn_w}(\eta_f - \eta)^{p-2}. \quad (149)$$

Note that the contributions of Eqs. 148 and 149 are of the same order and that the contribution of Eq. 147 is of higher order and can be neglected. Balancing powers of $\eta_f - \eta$ of Eqs. 145, 148, and 149, we indeed find a nontrivial solution, provided the balance:

$$\frac{1}{2}p + \frac{1}{2}pn_w - 1 + p - 1 = p - 1 \Rightarrow p = \frac{2}{n_w + 1}. \quad (150)$$

References

1. Chavent, G., Jaffré, J.: Mathematical models and finite elements for reservoir simulation: single phase, multiphase and multicomponent flows through porous media, vol. 17. Elsevier, New York (1986)
2. Dake, L.P.: Fundamentals of reservoir engineering. 1978 (1983)
3. Deng, L., King, M.J., et al.: Capillary corrections to buckley-leverett flow. In: SPE Annual Technical Conference and Exhibition. Society of Petroleum Engineers (2015)
4. Evje, S., Karlsen, K.H.: Viscous splitting approximation of mixed hyperbolic-parabolic convection-diffusion equations. Numer. Math. **83**(1), 107–137 (1999)
5. Karlsen, H.K., Brusdal, K., Dahle, H.K., Evje, S., Lie, K.-A.: The corrected operator splitting approach applied to a nonlinear advection-diffusion problem. Comput. Methods Appl. Mechan. Eng. **167**(3-4), 239–260 (1998)
6. Krushkov, S.N.: First-order quasilinear equations in several independent variables. Math. Sb. **123**, 228–255 (1970)
7. LeVeque, R.J.: Numerical methods for conservation laws, vol. 3. Springer, New York (1992)
8. Ling, K.: Fractional flow in radial flow systems: a study for peripheral waterflood. J. Petrol. Explor. Product. Technol. **6**(3), 441–450 (2016)
9. Martin, B.: Imperial college lectures. In: Petroleum engineering, the-volume 2: reservoir engineering, vol. 2. World Scientific Publishing Company, Singapore (2017)
10. Oleinik, O.A.: Discontinuous solutions of non-linear differential equations. Uspekhi Matematicheskikh Nauk **12**(3), 3–73 (1957)
11. Rapoport, L.A., Leas, W.J., et al.: Properties of linear waterfloods. J. Petrol. Tech. **5**(05), 139–148 (1953)
12. Smoller, J.: Shock waves and reaction—diffusion equations, vol. 258. Springer Science & Business Media, New York (2012)
13. Van Dyke, M.: Perturbation methods in fluid mechanics, vol. 136. Academic Press, New York (1964)
14. Henry, J., et al.: Welge a simplified method for computing oil recovery by gas or water drive. J. Petrol. Tech. **4**(04), 91–98 (1952)
15. Yortsos, Y.C.: Stability of displacement processes in porous media in radial flow geometries. Phys. Fluids **30**(10), 2928–2935 (1987)
16. Yortsos, Y.C., Fokas, A.S., et al.: An analytical solution for linear waterflood including the effects of capillary pressure. Soc. Pet. Eng. J. **23**(01), 115–124 (1983)